Assignment 5

Modes in Rectangular Waveguides

ELG 3106 - Electromagnetic Engineering

Fall 2023

School of Electrical Engineering and Computer Science

University of Ottawa

Tristan Ruel 300272156

December 6th, 2023

Index

Figure 1.0 - Value of Beta (rad/s) versus Frequency (MHz)……..7
Figure 2.0 - Simulation of the Mode TE10 Showing Power Component Sz…….……..10
Figure 2.1 - Simulation of the Mode TE10 Showing E(x,y)…….……...10
Figure 3.0 - Simulation of the Mode TE11 Showing Power Component Sz……...11
Figure 3.1 - Simulation of the Mode TE11 Showing E(x,y)……12
Figure 3.2 - Simulation of the Mode TE21 Showing Power Component Sz……...12
Figure 3.3 - Simulation of the Mode TE21 Showing E(x,y)……13
Figure 3.4 - Simulation of the Mode TM11 Showing Power Component Sz……...13
Figure 3.5 - Simulation of the Mode TM11 Showing H(x,y)……..14
Figure 3.6 - Simulation of the Mode TM21 Showing Power Component Sz……...14
Figure 3.7 - Simulation of the Mode TM21 Showing H(x,y)……..15

Executive Summary

This assignment offered an in-depth analysis of waveguiding in uniform metal-walled waveguides, focusing on the study of various wave modes and their behaviours within these structures. Structured into three distinct parts, each section concentrated on a different aspect of waveguide analysis, blending theoretical concepts with practical simulations. The theoretical framework was based on the homogeneous wave equations for a metal tube waveguide filled with a dielectric material, incorporating specific assumptions about the waveguide's dimensions and operating frequency to yield realistic results.

Part I concentrated on analyzing the dispersion relation and its correlation with frequencies ranging from 0 GHz to 10 GHz, utilizing the Module 8.5 applet to determine cutoff frequencies and calculate Beta (β) for various modes, which led to the creation of a Beta versus Frequency plot.

Part II aimed at verifying the accuracy of E(x, y) and Sz figures, merging theoretical equations with practical simulations to deepen the understanding of wave behaviour.

Part III presented simulation results for power density and electrical field plots across all degenerative modes, revealing the distinct characteristics of TE and TM modes, as well as their power densities and field configurations, and highlighting the uniformity in dispersion relations irrespective of specific field configurations.

This assignment emphasized the orthogonality of TE and TM modes, ensuring the independence of each mode's power and characteristics, and noted the consistent dispersion relations across modes, highlighting that waveguide behavior is influenced by general properties like geometric dimensions and mode numbers.

Introduction

This assignment delves into the intricate world of waveguiding in uniform metal-walled waveguides, focusing on the analysis and simulation of various wave modes within these structures. Our journey begins with a theoretical framework, laying the foundation for understanding the propagation of electromagnetic waves in waveguides. We explore the homogeneous wave equations for a waveguide characterized as a metal tube embedded with a dielectric material. The propagation within this waveguide will be examined through the equation:

$$E(x,y,z;t) = \Re e\left\{E(x,y)e^{-\gamma z}e^{jwt}\right\} and\ H(x,y,z;t) = \Re e\left\{H(x,y)e^{-\gamma z}e^{jwt}\right\}$$

Our investigation is grounded in specific assumptions for our simulations, including the dimensions of the waveguide and the operating frequency. These assumptions provide a realistic context for our analysis, ensuring that the results are applicable and meaningful.

In Part I of the assignment, we focus on the dispersion relation and its correlation with frequencies ranging from 0 GHz to 10 GHz. Using the Module 8.5 applet, we determine cutoff frequencies for various modes and calculate Beta (β) in radians per second for each mode. This analysis allows us to create a detailed plot of Beta versus Frequency, illustrating the relationship between these two critical parameters.

Part II shifts our attention to verifying the accuracy of E(x, y) and S_z figures displayed in the Module 8.5 applet. This involves expressing E(x,y) and S_z through a series of equations and conducting detailed calculations. The results of this verification process are presented through simulations, providing a visual representation of our findings.

Finally, Part III presents the simulation results of power density and electrical field plots for all degenerative modes. These simulations reveal the distinct characteristics of TE and TM modes and their respective power densities and field configurations. We also discuss the uniformity in dispersion relations across different modes, highlighting fundamental principles of waveguide behaviour.

Theory

In our theory discussion, we will focus on the homogeneous wave equations for a uniform waveguide. This waveguide is characterized as a metal tube filled with a dielectric material. We will describe the propagation within this waveguide using the following equation:

$$E(x,y,z;t) = \Re e\left\{E(x,y)e^{-\gamma z}e^{jwt}\right\} \; and \; H(x,y,z;t) = \Re e\left\{H(x,y)e^{-\gamma z}e^{jwt}\right\}$$

Where gamma:

$$\gamma = \alpha + j\beta = \sqrt{h^2 - k^2}$$

Where:

$$h^2 = k_r^2 + k_y^2$$

With:

$$k_x = \frac{m\pi}{a} \; and \; k_y = \frac{n\pi}{b}$$

Where the cut-off frequency is given by:

$$f_c = \frac{h}{\sqrt{2\pi\sqrt{\mu\varepsilon}}}$$

For wavenumber:

$$\beta = \left(\frac{2\pi}{c}\right)\sqrt{f^2 - f_c^2}$$

Where the phase speed of the mode and wavelength in the guide are given by:

$$u_p = \frac{u}{\sqrt{1-\left(\frac{f_c}{f}\right)^2}} \; and \; \lambda_g = \frac{\lambda}{\sqrt{1-\left(\frac{f_c}{f}\right)^2}}$$

We will use the following assumptions in our simulations:

a = 0.05 m

a/b = 2.0

Frequency = $1.0*10^{10}$ Hz

$\varepsilon_r = 1$

$\mu_r = 1$

*The entirety of this section was created using the works of Dr. H. Schrimer. (Schriemer, 2023)

Part I

In the first part of our assignment, we aimed to determine how the dispersion relation correlates with frequencies between 0 GHz and 10 GHz. To calculate Beta (β), it was necessary to utilize the Module 8.5 applet, which assists in identifying the cutoff frequencies. By utilising the Mode Selector for all modes to determine the cutoff frequencies. Once we determined the cutoff frequencies for each of the seven modes, we could then apply the following formula to calculate Beta in radians per second:

$$\beta = \left(\frac{2\pi}{c}\right)\sqrt{f^2 - f_c^2}$$

Next, we obtain the calculations for Beta in each mode:

For TE_{10}, where f_c = 3 GHz and f = 10 GHz:

$$\beta = \left(\frac{2\pi}{c}\right)\sqrt{f^2 - f_c^2} = \left(\frac{2\pi}{3*10^8}\right)\sqrt{\left(10 * 10^9\right)^2 - \left(3 * 10^9\right)^2} = 199.7925\, rad/s$$

For TE_{01} & TE_{20}, where f_c = 6 GHz and f = 10 GHz:

$$\beta = \left(\frac{2\pi}{c}\right)\sqrt{f^2 - f_c^2} = \left(\frac{2\pi}{3*10^8}\right)\sqrt{\left(10 * 10^9\right)^2 - \left(6 * 10^9\right)^2} = 167.5516\, rad/s$$

For TE_{11} & TM_{11}, where f_c = 6.71 GHz and f = 10 GHz:

$$\beta = \left(\frac{2\pi}{c}\right)\sqrt{f^2 - f_c^2} = \left(\frac{2\pi}{3*10^8}\right)\sqrt{\left(10 * 10^9\right)^2 - \left(6.71 * 10^9\right)^2} = 155.2904\, rad/s$$

For TE_{21} & TM_{21}, where f_c = 8.49 GHz and f = 10 GHz:

$$\beta = \left(\frac{2\pi}{c}\right)\sqrt{f^2 - f_c^2} = \left(\frac{2\pi}{3*10^8}\right)\sqrt{\left(10 * 10^9\right)^2 - \left(8.49 * 10^9\right)^2} = 110.6663\, rad/s$$

For TE_{30}, where f_c = 9 GHz and f = 10 GHz:

$$\beta = \left(\frac{2\pi}{c}\right)\sqrt{f^2 - f_c^2} = \left(\frac{2\pi}{3*10^8}\right)\sqrt{\left(10 * 10^9\right)^2 - \left(9 * 10^9\right)^2} = 91.2925\, rad/s$$

The above allows us to obtain the values required to plot the Betas in the following Figure 1.0:

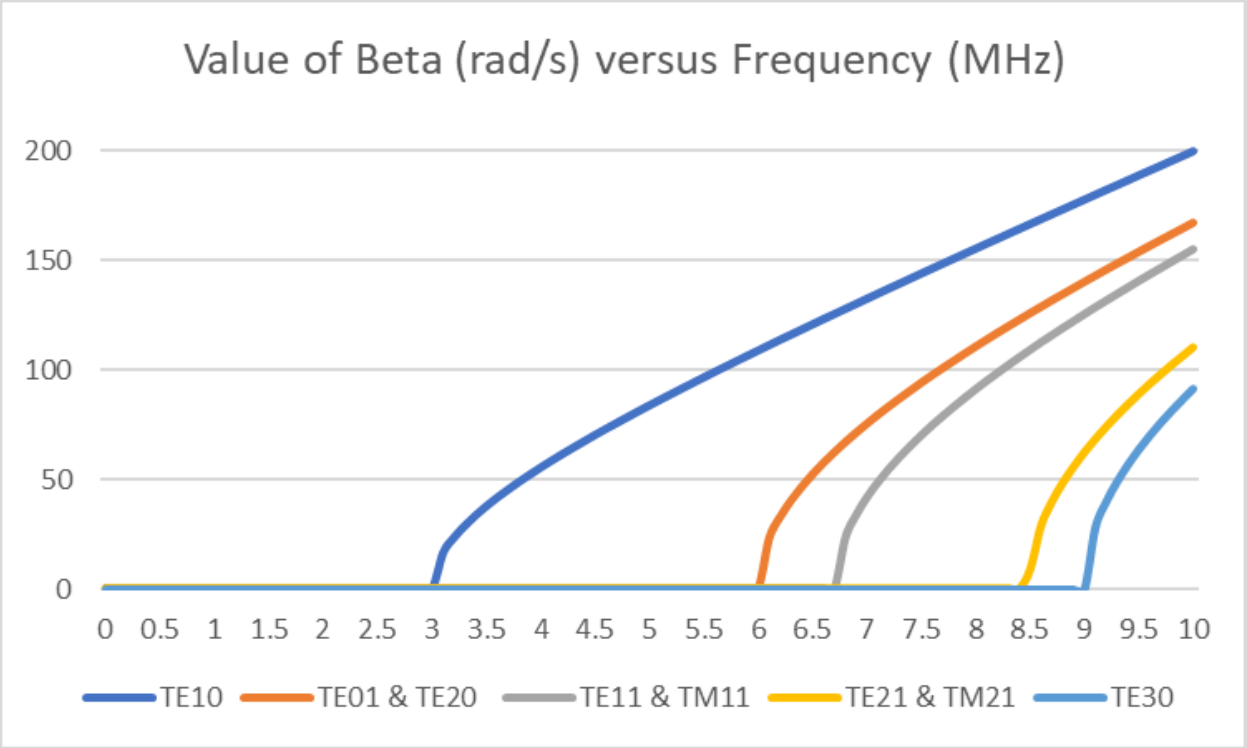

Figure 1.0 - Value of Beta (rad/s) versus Frequency (MHz)

The formula utilised for the excel graph is as follows:

=(2*PI/(3*10^8))*SQRT(((B4*10^9)^2)-((C2*10^9)^2))

Where, C2 is the value of the cutoff frequency and where B4 is the value of the frequency. For ease, the input values are between 0 and 10, and are subsequently multiplied by 10^9.

The above Figure 1.0 illustrates the theoretical concepts reflected in a graph. Notably, the graph lines only commence when the frequency on the X-axis surpasses the cut-off frequency for each mode. Post the cut-off frequency, the propagation constant β escalates with frequency, aligning well with the theoretical expectations.

A notable observation is the merging of some lines, indicative of different modes (such as TE11 & TM11, TE20 & TE01, TE21 & TM21) sharing identical cut-off frequencies. These modes are termed 'degenerate modes', characterized by similar field pattern periodicities, albeit with varying orientations of electric and magnetic fields.

The graph was created using Excel, where the steps were straightforward:

1- Define a range of frequencies in a column, incrementally listed

2- Apply the Beta formula to each mode, adjusting the cut-off frequency as determined in the simulations.

3- Create a chart with the frequency on the x-axis and Beta on the y-axis.

Part II

In the following section, our objective is to verify the accuracy of the E(x, y) and S_z figures displayed in the Module 8.5 applet. To achieve this, we must express E(x,y) and S_z using a series of equations. Below are the detailed calculations and explanations for deriving these equations.

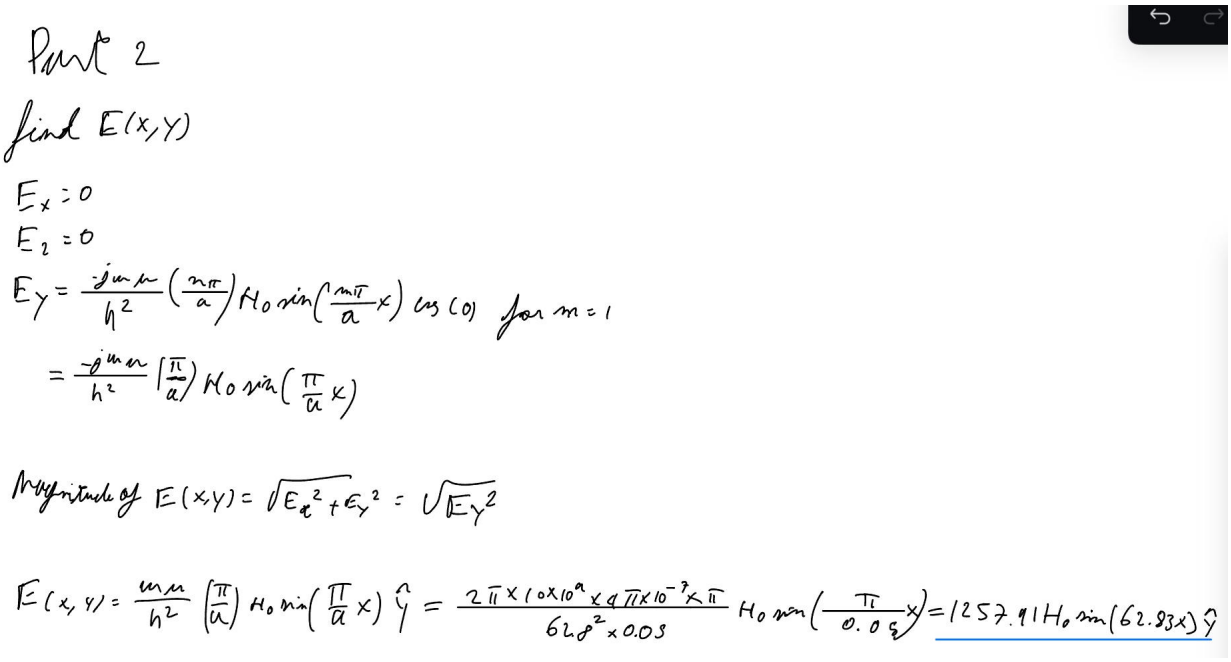

Finding $H(x,y)$

$H_y = 0$

$H_x = \frac{\gamma}{h^2}\left(\frac{m\pi}{a}\right) H_0 \sin\left(\frac{m\pi}{a}x\right) \cos(0)$

$H_z = H_0 \cos\left(\frac{m\pi}{a}x\right) \cos\left(\frac{n\pi}{b}y\right)$

$H(x,y) = H_x = \frac{\gamma}{h^2}\left(\frac{\pi}{a}\right) H_0 \sin\left(\frac{\pi}{a}x\right)\hat{x}$

$\gamma = j\beta = j(199.7925)$

$H(x,y) = \frac{j(199.7925)\times\pi}{62.8^2 \times 0.05} H_0 \sin\left(\frac{3.14}{0.05}x\right) = j3.183 H_0 \sin(62.8x)$

Finding the power component of S_z

$S_z = \tilde{E}(x,y)\hat{y} \times \tilde{H}(x,y)\hat{x}$

$= \frac{w\mu}{h^2}\left(\frac{\pi}{a}\right) H_0 \sin\left(\frac{\pi}{a}x\right)\hat{y} \times \frac{\gamma}{h^2}\left(\frac{\pi}{a}\right) H_0 \sin\left(\frac{\pi}{a}x\right)\hat{x}$

$= \frac{\gamma w\mu}{h^4}\left(\frac{\pi}{a}\right)^2 H_0^2 \sin\left(\frac{\pi}{a}x\right)^2 \hat{z}$

$= \frac{j199.7925 \times 4\pi\times10^{-7}}{62.831^4} 62.831^2 H_0^2 \sin(62.831x)^2 \hat{z}$

$= j6.359\times10^{-8} H_0^2 \sin(62.831x)^2 \hat{z}$

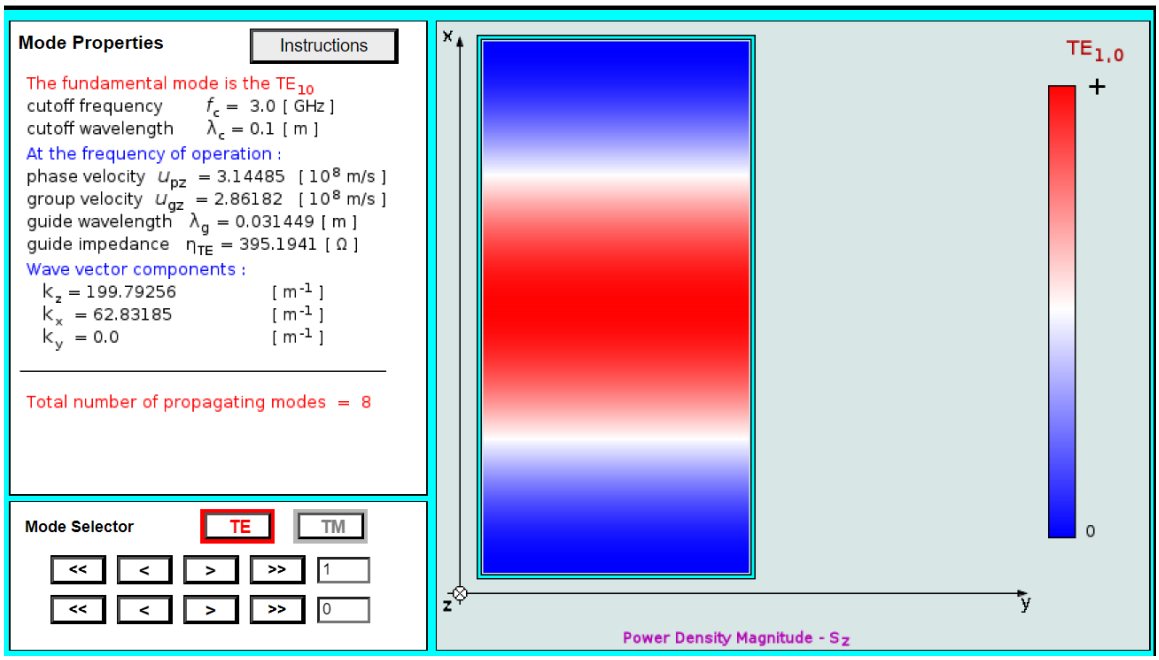

Figure 2.0 - Simulation of the Mode TE_{10} Showing Power Component S_z

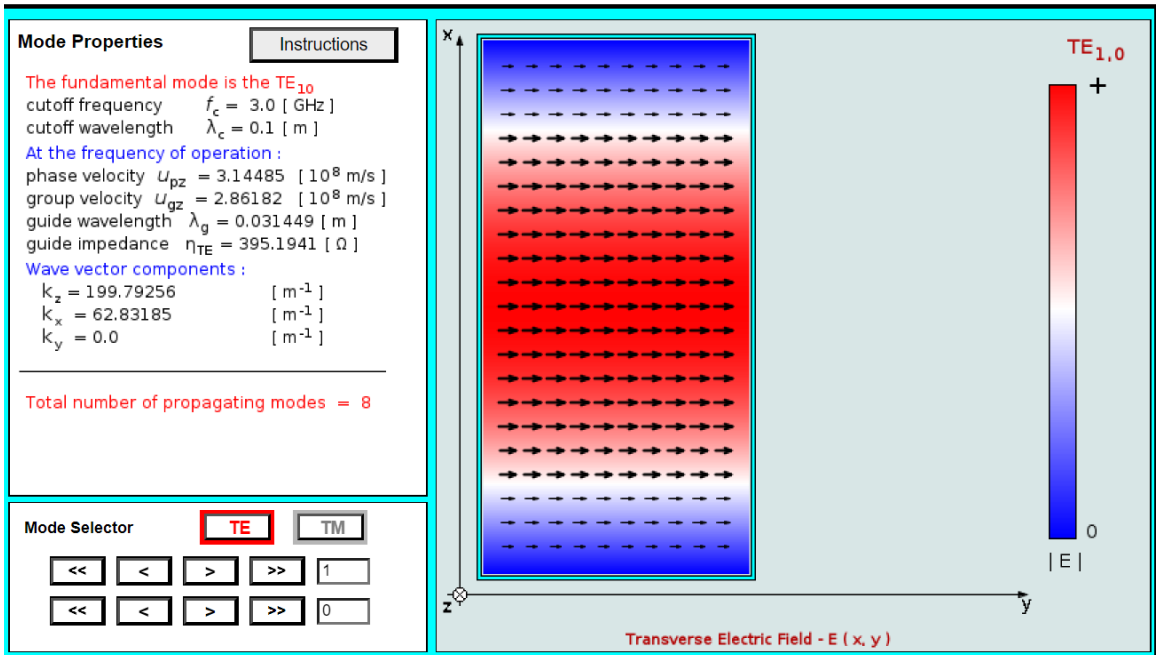

Figure 2.1 - Simulation of the Mode TE_{10} Showing E(x,y)

In Figure 2.0's, the color map represents the power density magnitude, S_z, throughout the waveguide. The colour intensity in this depiction corresponds to the power density level. Given that S_z is directly related to $\sin^2(\pi x/a)$, we expect the power density to peak at the waveguide's

center (where x=a/2) and to be minimal (zero) at the edges (where x=0 or x=a), mirroring the sine wave's nodes.

Figure 2.1's colour map aligns with our Transverse Electric Field, as indicated by the arrows pointing in the +y direction, which is also reflected in our equation. Additionally, the colour map shows the electric field's magnitude: at the waveguide's center (where x is half of a), the field is strongest, shown in red, and it's weakest, depicted in blue, at the edges (where x=0 or x=a). This variation is in line with the sinusoidal pattern of $\sin(\pi x/a)$.

*This section was created using the works of the Module 8.5 app (F. Ulaby, 2020)

Part III

In the following section, we will show the simulation results of the power density and electrical field plots for all degenerative modes.

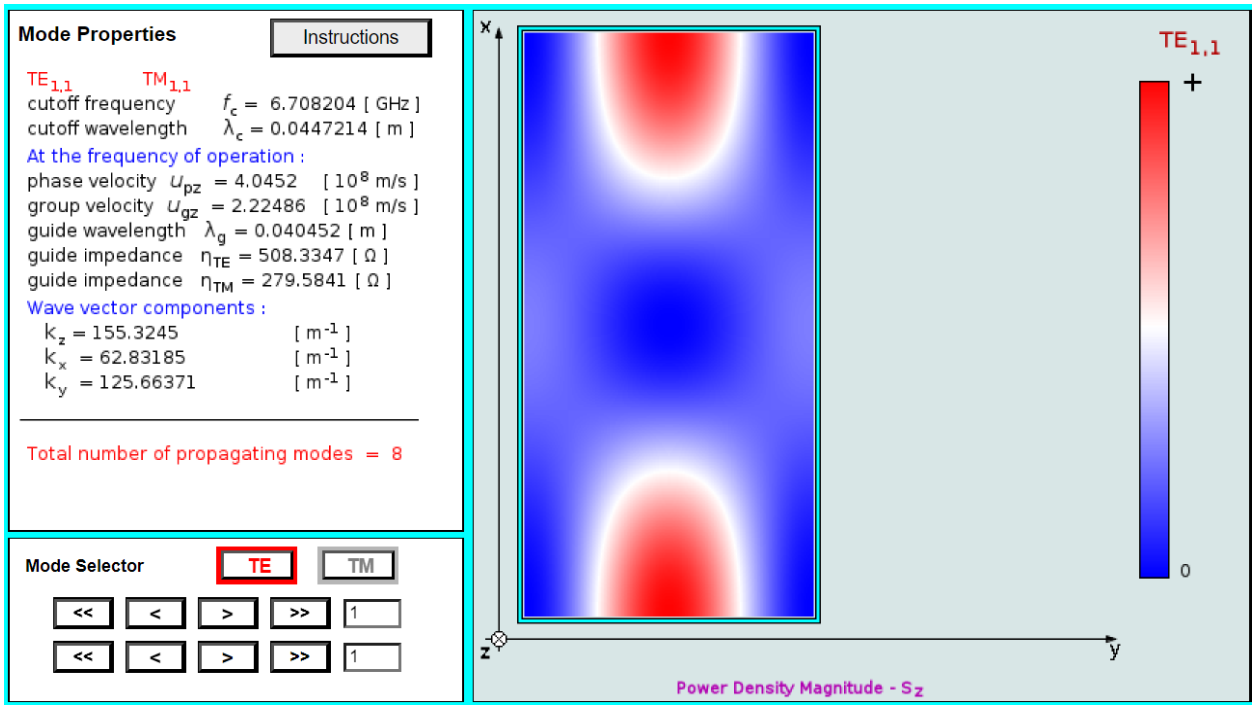

Figure 3.0 - Simulation of the Mode TE_{11} Showing Power Component S_z

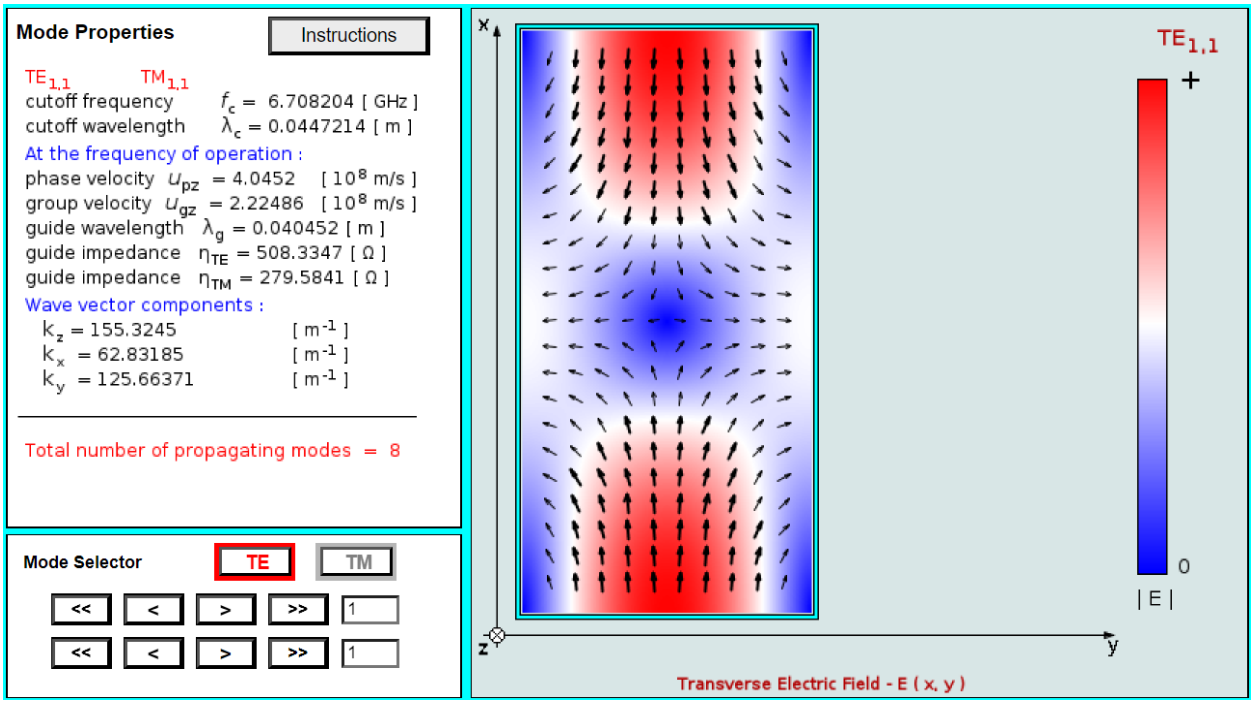

Figure 3.1 - Simulation of the Mode TE_{11} Showing E(x,y)

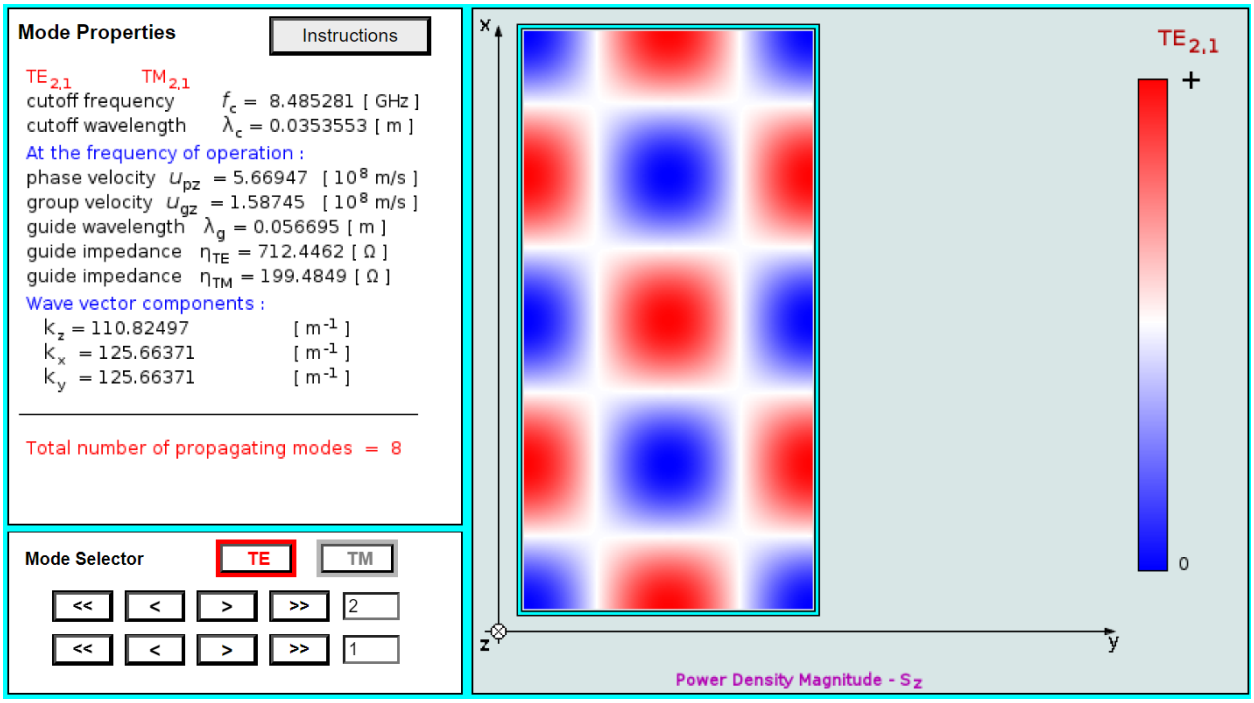

Figure 3.2 - Simulation of the Mode TE_{21} Showing Power Component S_z

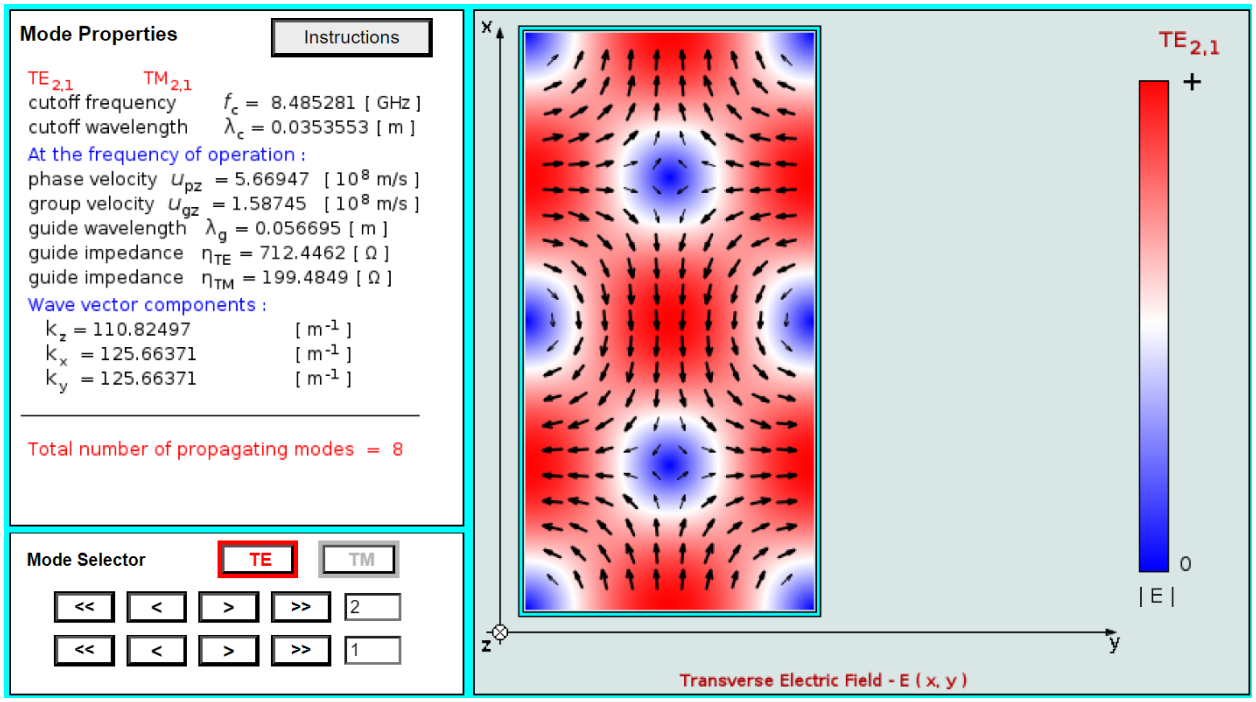

Figure 3.3 - Simulation of the Mode TE_{21} Showing E(x,y)

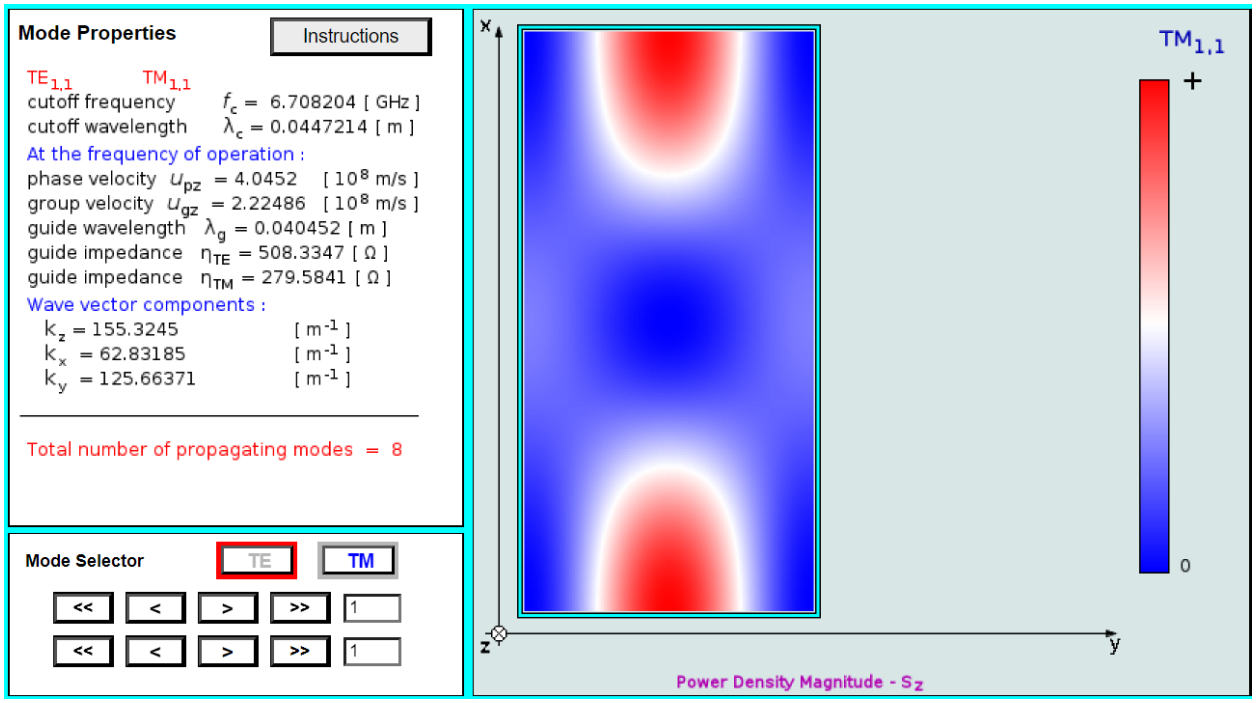

Figure 3.4 - Simulation of the Mode TM_{11} Showing Power Component S_z

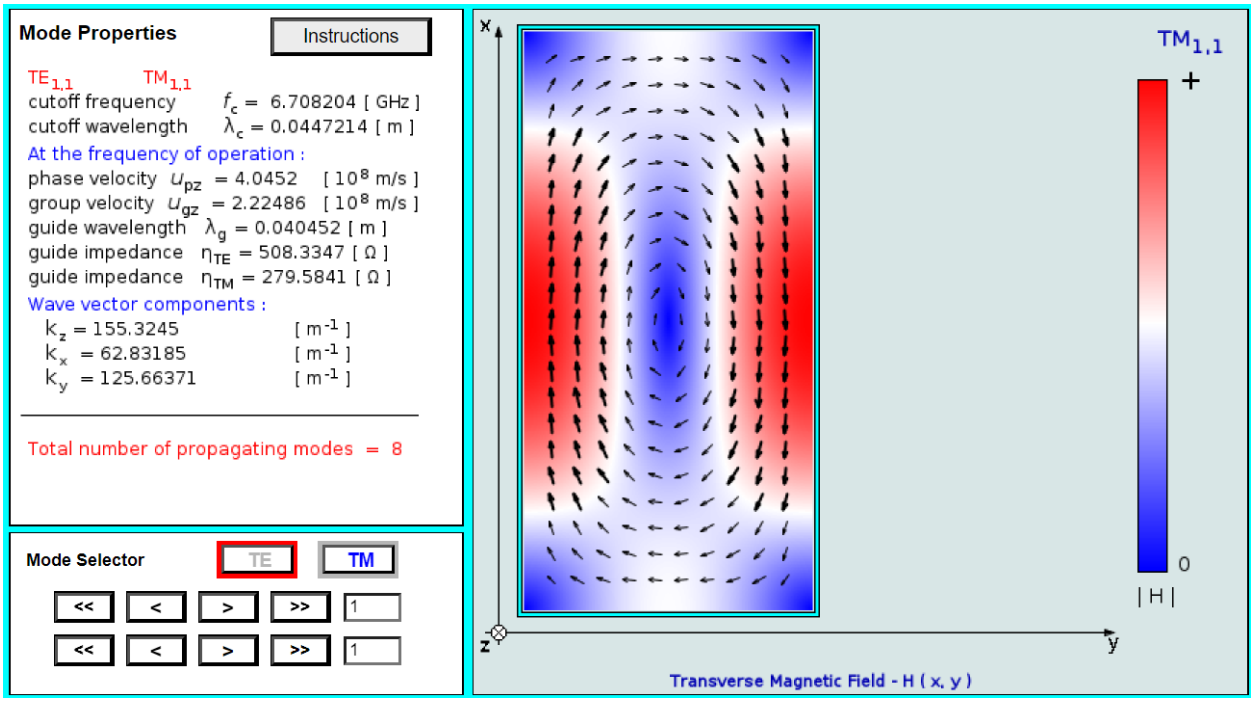

Figure 3.5 - Simulation of the Mode TM_{11} Showing H(x,y)

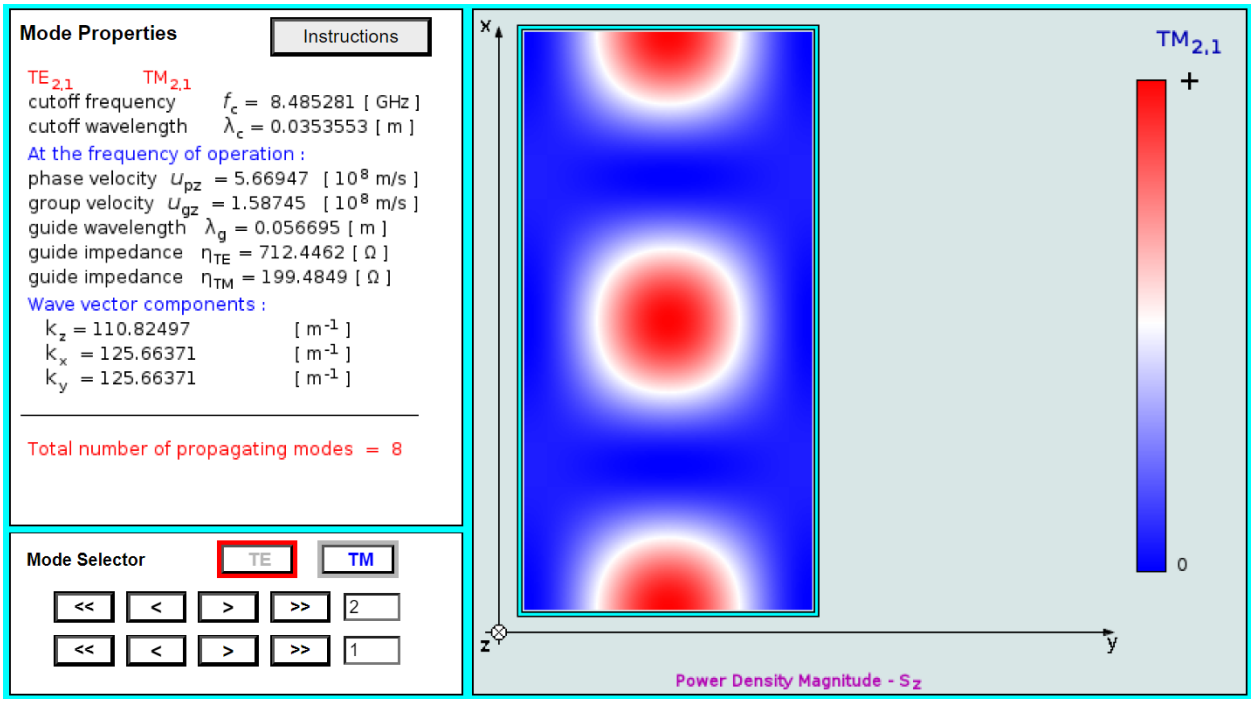

Figure 3.6 - Simulation of the Mode TM_{21} Showing Power Component S_z

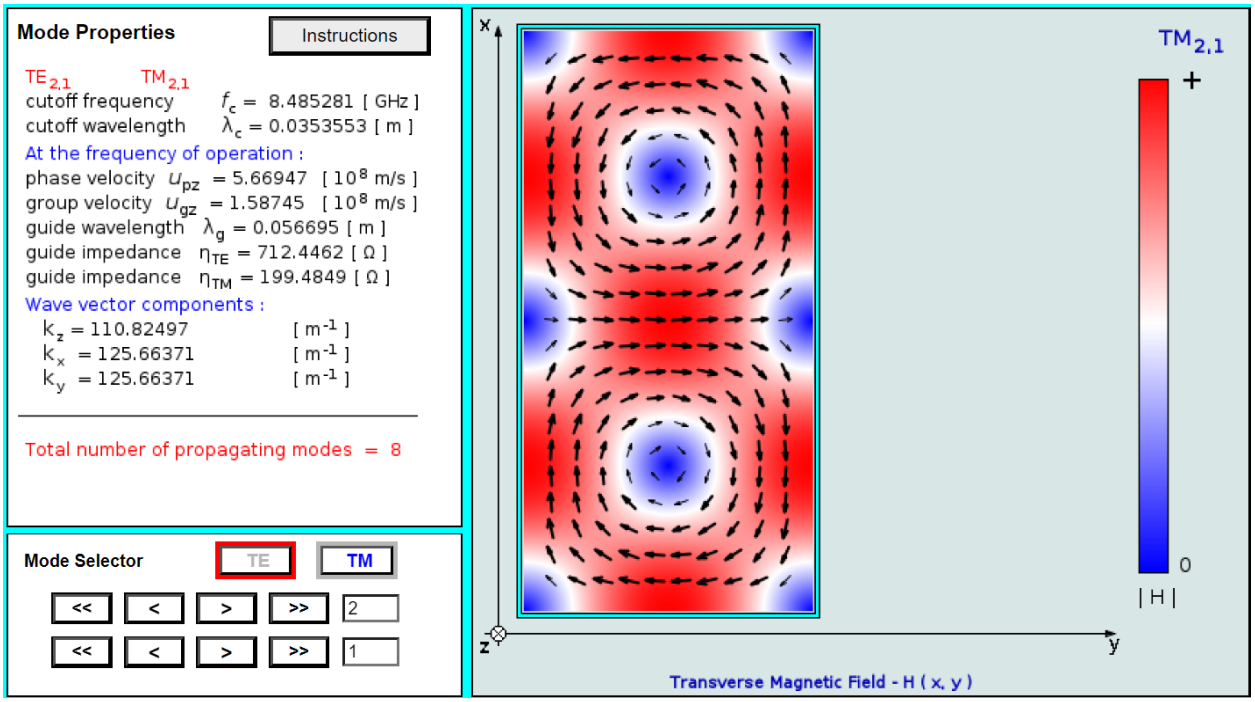

Figure 3.7 - Simulation of the Mode TM_{21} Showing H(x,y)

*This section was created using the works of the Module 8.5 app (F. Ulaby, 2020)

Discussion

In the above figures, it becomes evident that although the modes exhibit different power densities, there is no significant variation in their dispersion properties. The power densities of the modes are distinct due to the unique characteristics of the TE and TM modes. These differences stem from their respective electric and magnetic field configurations. The fields in TE and TM modes are orthogonal to each other, meaning they are positioned at right angles and do not influence each other. This orthogonality ensures that the power from one mode does not overlap or 'bleed' into the other, preserving the independence and purity of each mode's characteristics.

Despite these differences in power densities and field configurations, the dispersion relations of both modes remain unchanged. This consistent aspect of dispersion is crucial as it highlights a fundamental principle of waveguide behaviour. The dispersion relation, which is essential in understanding how the phase velocity of a wave mode varies with its frequency, is not dependent on the specific configurations of the electric or magnetic fields. Instead, it is determined by more general properties of the waveguide system. These include the geometric dimensions of the waveguide and the mode numbers (m and n), which represent the modes' specific characteristics in the waveguide. This universal aspect of the dispersion relation across different modes underscores the intrinsic properties of the waveguide that are independent of the particular field distributions within each mode.

Conclusion

As we conclude this comprehensive study on waveguiding in uniform metal-walled waveguides, several key insights emerge, reinforcing our understanding of electromagnetic wave propagation in these structures. Our journey through the theoretical framework, detailed simulations, and analytical evaluations has yielded a multi-faceted view of waveguide behaviour, especially focusing on the TE and TM modes.

In Part I, our exploration of the dispersion relation and its interplay with frequencies ranging from 0 GHz to 10 GHz underscored the complex nature of electromagnetic waves in waveguides. The use of the Module 8.5 applet was instrumental in calculating Beta (β) for various modes, providing a clear illustration of the intricate relationship between Beta and frequency. This foundational understanding set the stage for more detailed analyses in subsequent parts of the assignment.

Part II's focus on verifying the accuracy of E(x, y), and S_z figures through a series of equations and simulations demonstrated the practical application of theoretical principles. The visual representations from these simulations not only validated the theoretical models but also enhanced our comprehension of wave behaviour in a tangible manner.

The culmination of our study in Part III, where we examined the simulation results for power density and electrical field plots across all degenerative modes, revealed significant findings. The distinct power densities and field configurations of TE and TM modes highlighted the diversity within waveguide systems. Despite these differences, the uniformity in dispersion relations across these modes was a critical discovery. It reinforced the principle that waveguide behaviour, particularly the phase velocity variations with frequency, is predominantly determined by general properties like geometric dimensions and mode numbers, rather than specific field configurations.

References

- H. Schriemer, "Assignment 5," University of Ottawa, Ottawa, Ontario, Canada, Nov. 27, 2023
- F. Ulaby, "Module 8.5." University of Michigan, Dept. of EECS. [Online]. Available: https://em8e.eecs.umich.edu/jsmodules/ch2/mod2_3.html. Accessed on: Nov. 27, 2023.

Appendix
Figures

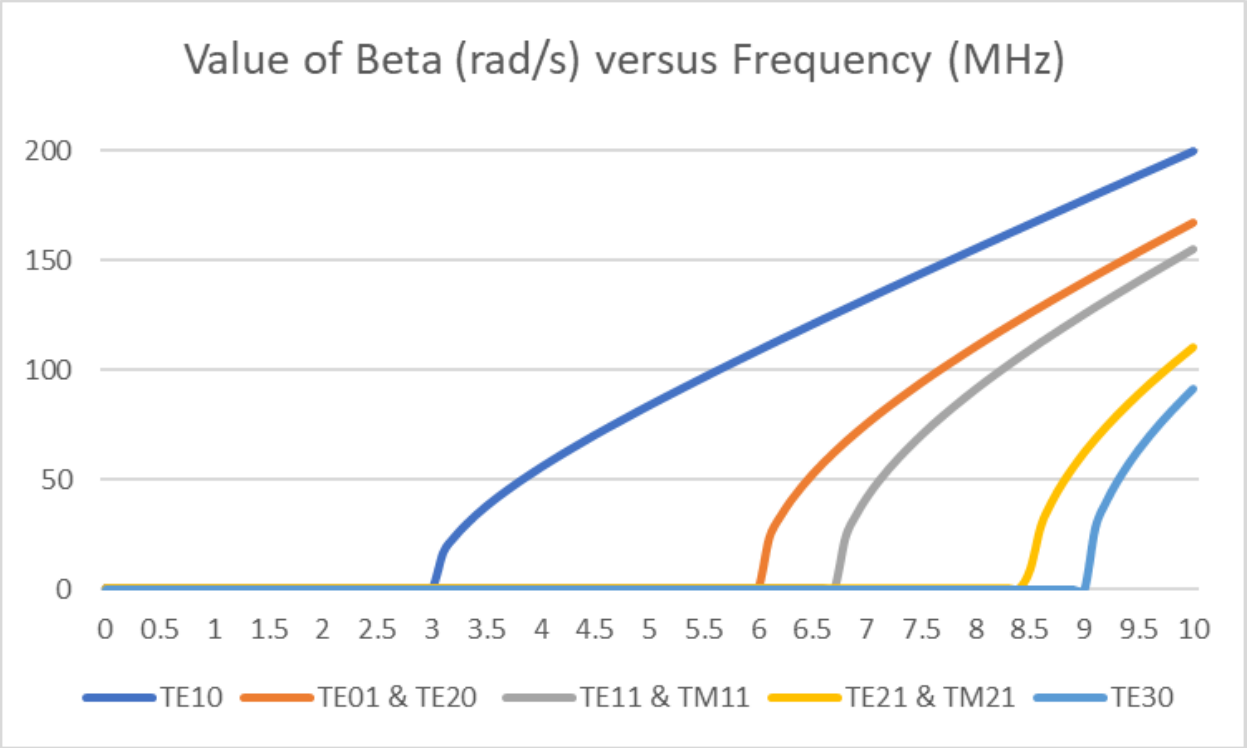

Figure 1.0 - Value of Beta (rad/s) versus Frequency (MHz)

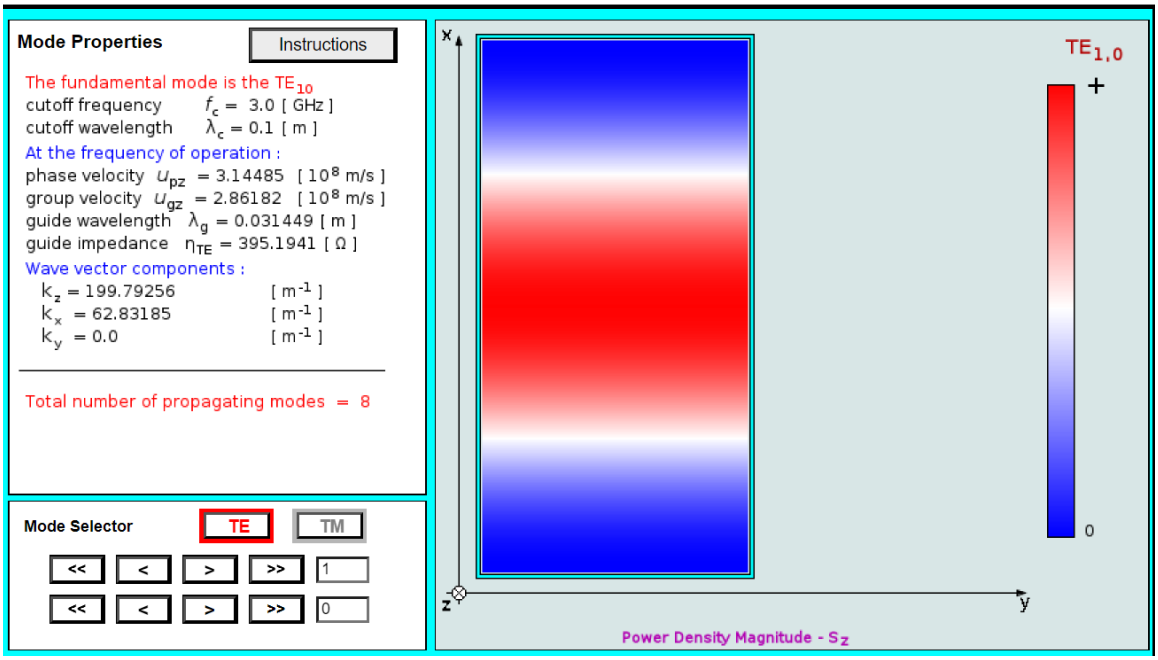

Figure 2.0 - Simulation of the Mode TE_{10} Showing Power Component S_z

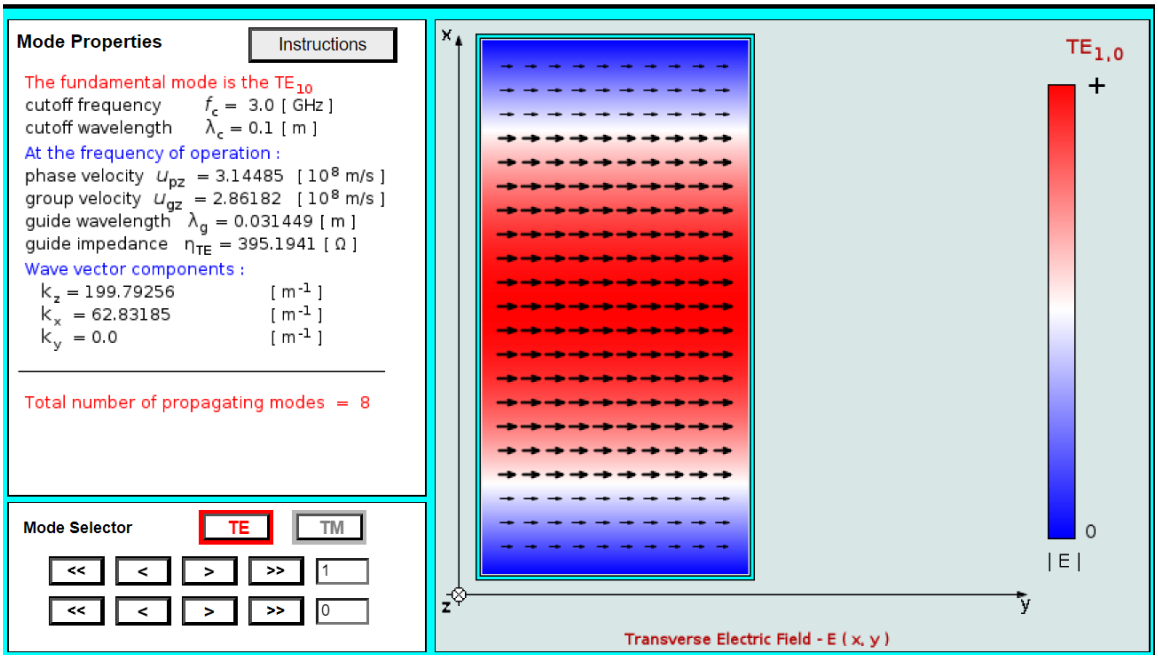

Figure 2.1 - Simulation of the Mode TE_{10} Showing E(x,y)

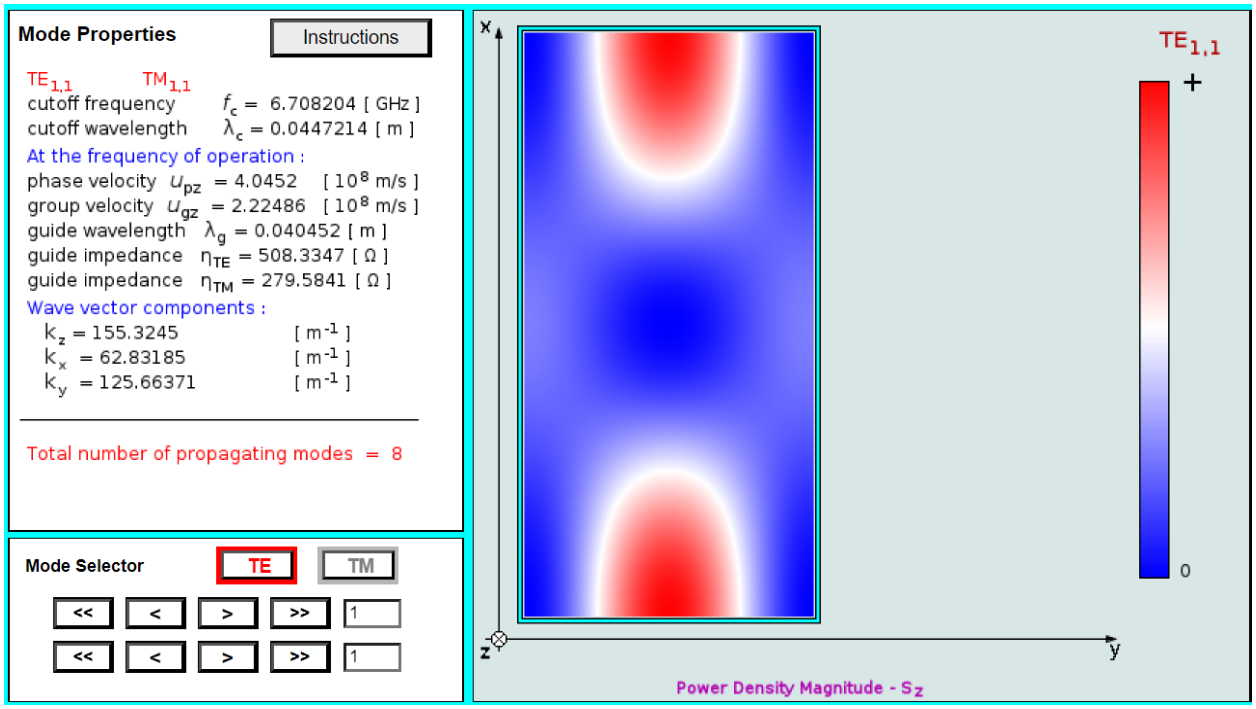

Figure 3.0 - Simulation of the Mode TE_{11} Showing Power Component S_z

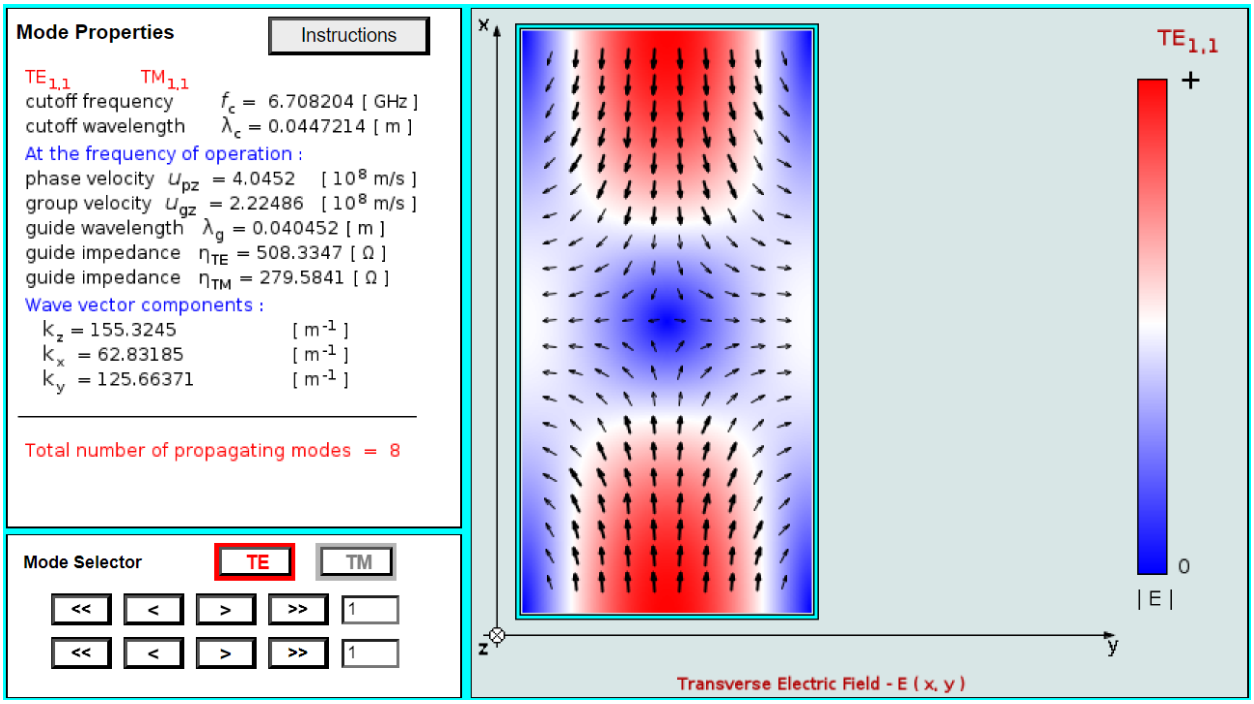

Figure 3.1 - Simulation of the Mode TE_{11} Showing E(x,y)

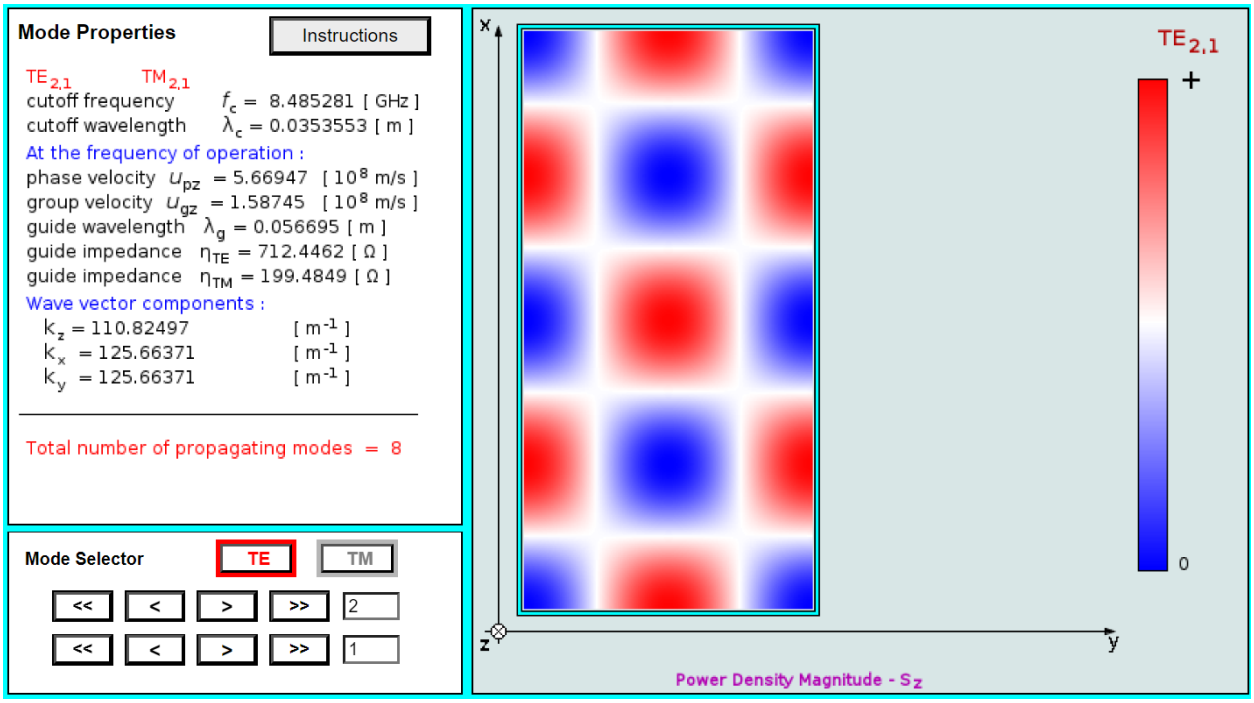

Figure 3.2 - Simulation of the Mode TE_{21} Showing Power Component S_z

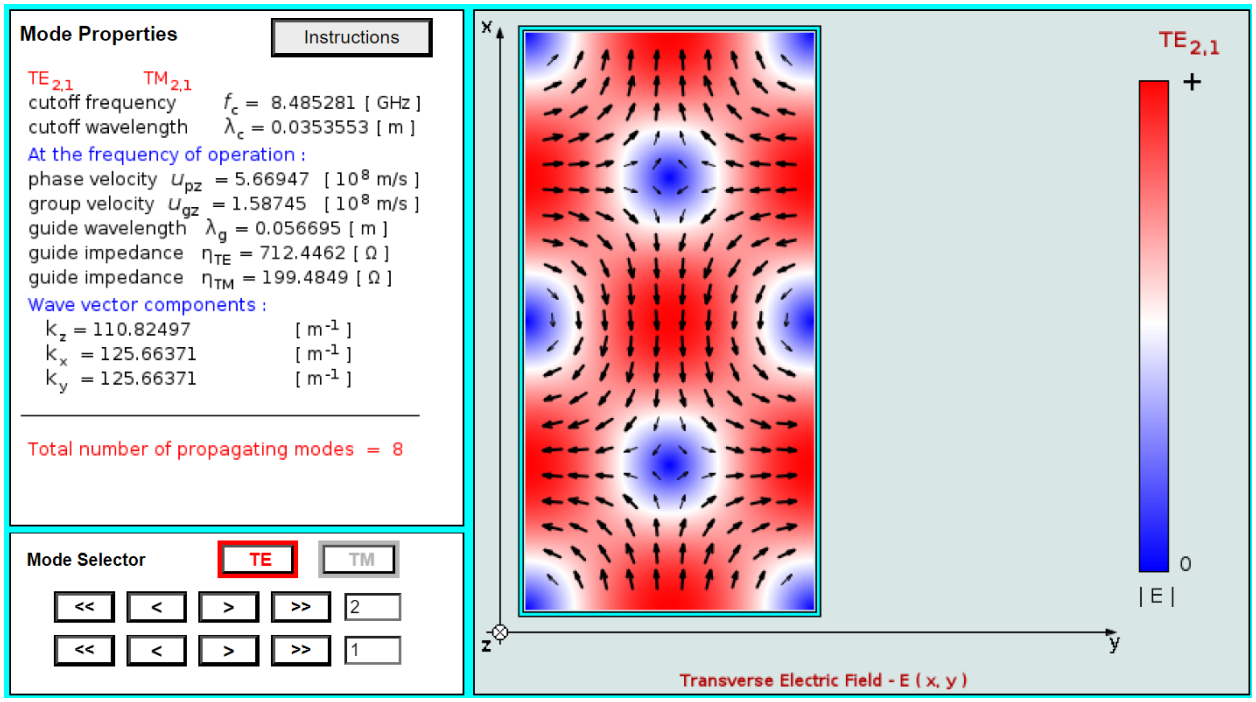

Figure 3.3 - Simulation of the Mode TE_{21} Showing E(x,y)

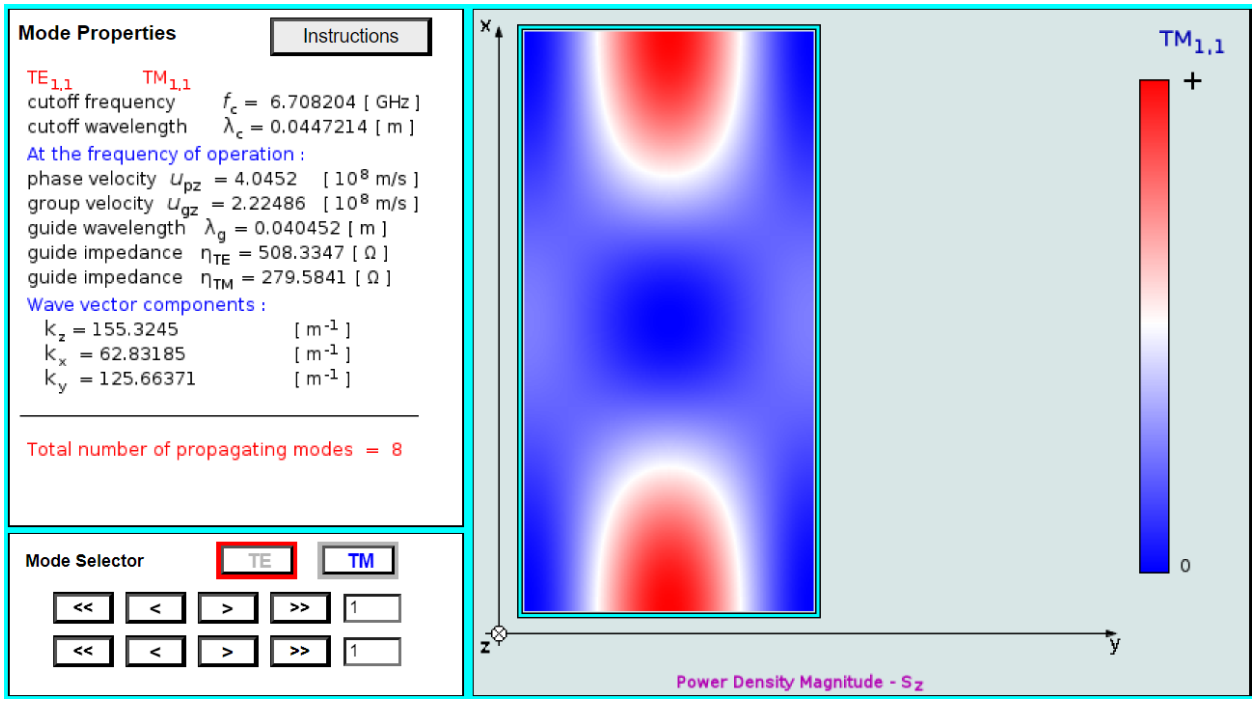

Figure 3.4 - Simulation of the Mode TM_{11} Showing Power Component S_z

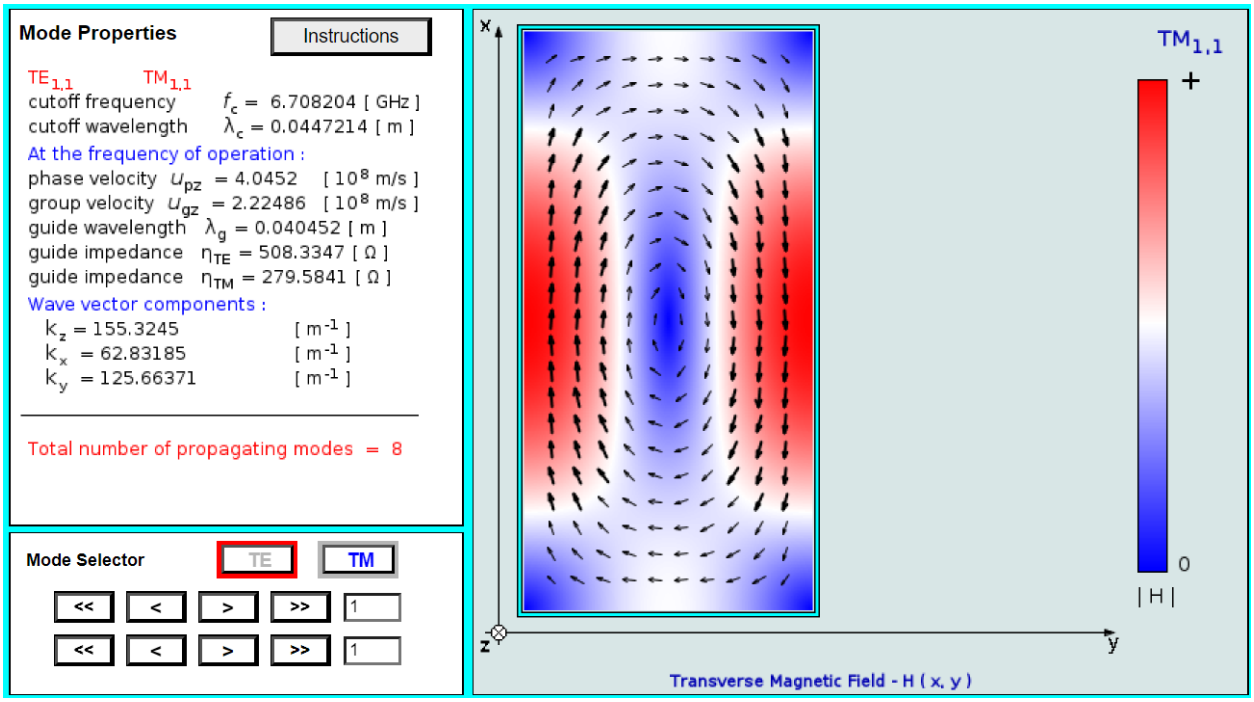

Figure 3.5 - Simulation of the Mode TM_{11} Showing H(x,y)

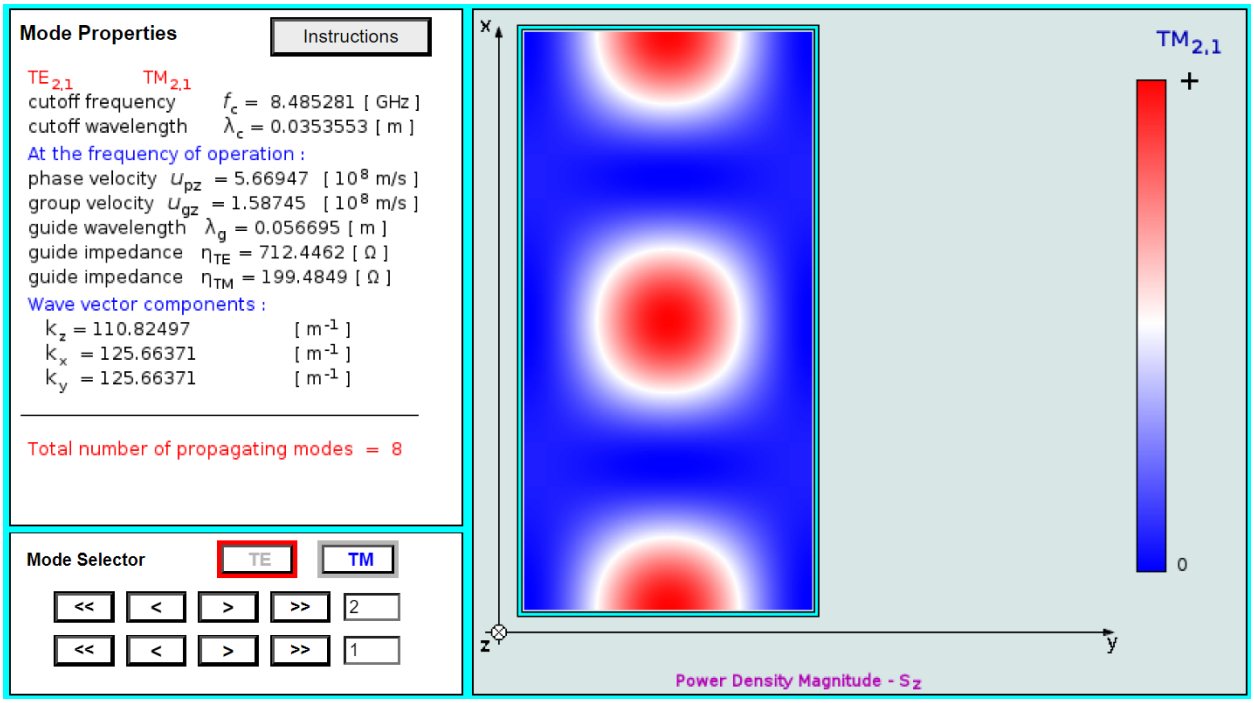

Figure 3.6 - Simulation of the Mode TM_{21} Showing Power Component S_z

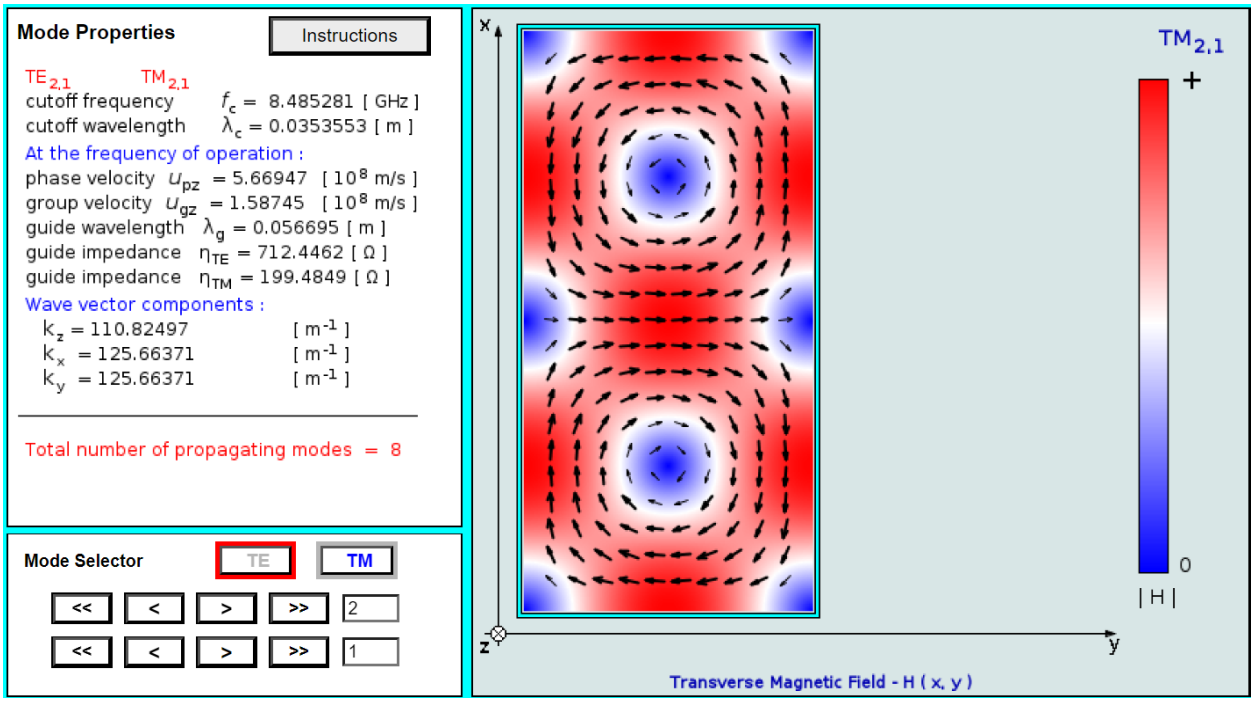

Figure 3.7 - Simulation of the Mode TM_{21} Showing H(x,y)

*This section was created using the works of the Module 8.5 app (F. Ulaby, 2020)

Code Appendix

This assignment did not require any computational methods.